Transactions of the TSME (2017) Vol. 5, No. 2, 106-118
Journal of Research and Applications in Mechanical Engineering

ISSN 2229-2152 print
DOI: 10.14456/jrame.2017.10

*Research Article*

# EFFECT OF INCLINED PINS ON FLOW AND HEAT TRANSFER CHARACTERISTICS FOR SINGLE ROW IN RECTANGULAR CHANNEL

**P. Narato**[1]
**M. Wae-hayee**[1]
**M. Z. Abdullah**[2]
**C. Nuntadusit**[1,*]
[1]*Department of Mechanical Engineering, Faculty of Engineering, Prince of Songkla University, Hatyai, Songkhla, 90112, Thailand*
[2]*School of Mechanical Engineering, Engineering Campus, Universiti Sains Malaysia, Nibong Tebal, Penang, 14300, Malaysia*

**ABSTRACT:**
*The aim of this research is to study the flow and heat transfer characteristics for a row of inclined pins on heat transfer surface. Cylindrical pins having 10 mm diameter (D) were mounted on heat transfer surface in the wind tunnel with inline arrangement. The pin height (H) and pin-to-pin distance (S) were fixed at H=2D, and S=2D, respectively. The effect of pin inclination angle were investigated at* $\theta = 30^o, 45^o, 60^o, 90^o, 120^o, 135^o$, *and* $150^o$. *For all experiments, the Reynolds number of air flow was fixed at Re=5,200. The results show that the pin inclination angle* $\theta = 30^o, 45^o$ *and* $60^o$ *enhances the heat transfer on the upstream and downstream of the pin row as compared to pin angle* $\theta = 90^o$. *The pin inclination angle* $\theta = 120^o$ *and* $135^o$ *somewhat improve the heat transfer region behind the pins. However, the pin inclination angle* $\theta = 150^o$ *gives the lowest heat transfer rate on overall surface. The mechanism of heat transfer enhancement and deterioration for inclined pin can be explained with secondary counter-rotating vortices and wake flow behind the pins.*

**Keywords:** *Cylindrical pin, Flow and heat transfer characteristics, Pin inclination angle, CFD.*

## 1. INTRODUCTION

The pin arrays are typically used for heat transfer enhancement on surface in a variety of engineering applications, such the cooling of gas turbine blades, electronic devices and enhancing heat transfer in compact heat exchangers. The pins used in turbine blade cooling have pin height-to-diameter ratio H/D between 0.5 and 4 [1]. The array of pins which have pin height-to-diameter ratio H/D more than 8 are used in the heat exchanger. Short pins with small pin height-to-diameter ratio H/D less than 0.5 are applied in certain types of plate-fin heat exchangers. The heat transfer enhancements using pin arrays occur due to two factors; first factor is increasing of heat transfer surface of pin and second factor is increasing of heat transfer coefficient on end wall of pins [2]. The heat transfer enhancement of pins with high height is dominated by the increasing of pin surface area, while the end-wall effect is not significant [3]. However, the mechanism of heat transfer enhancement of short pins is larger than addition of heat transfer surface on pins due to thermal boundary disturbance on end wall. Pin arrays are generally cylindrical in shape protruding from the heat transfer surface. The heat transfer fluid is forced to flow through the array of pins for cooling.

Chyu et al. [2] used surface flow visualization technique to investigate the flow behavior on a flat plate with cylindrical pin attachment. The horseshoe vortex is generated on end wall in front of the pin. A Pair of strong

* Corresponding author: C. Nuntadusit
E-mail address: chayut.n@psu.ac.th

rotating motion and separate flow is observed behind the pin. The separate flow disturbed the boundary layer and promoted the turbulent flow behind the pin. This will affect to the heat transfer enhancement behind the pin. Chyu [4] studied the effect of pin shape on heat and mass transfer enhancement focusing only for mounting pin normal to the heat transfer surface. Inline and staggered arrays with and without base fillet were studied. The heat and mass transfer performance of straight cylinder (without fillet cylinder) with staggered arrays was higher than that of fillet cylinders. Pandit et al. [5] presented 3-dimensional partial pin with staggered arrays of circular, triangular, hexagonal and diamond shapes on heat transfer enhancement in channel with rectangular cross section. The result revealed that diamond shape pin fin increased higher heat transfer than other all shapes. Rao et al. [6] examined pressure loss and heat transfer characteristics of pins with dimples employed on surface in a channel flow. The pins with dimple surface enhanced heat transfer performance by 19% as compared with pins with smooth surface. Wan et al. [7] present the heat transfer characteristics of an array of jet impingement on a flat plate and plates roughened with inline/staggered square pin-fins. The Reynolds numbers from 15,000 to 35,000 were studied for comparison of the heat transfer characteristics. The overall heat transfer rate of the jet impingement on the inline pin-fin plate can be increased by up to 34.5% compared with the jet impingement on the flat plate. The inline square pin-fin on impingement plate showed better heat transfer performance than that on the staggered square pin-fin on impingement plate. Axtmann et al. [8] studied heat transfer characteristics on surface with different pin fin arrays. The configurations included short and long elements. The Reynolds number of air flow (based on the pin fin diameter) varies from 3,000 to 30,000. The short pin fin provides higher heat transfer enhancement on the endwall. The shorter pin fin arrays provided better heat transfer enhancement than longer pin fin arrays. Xie et al. [9] presented heat transfer characteristics on the tip cap surface of U-shaped cooling channel with pin-fin-dimple/protrusion and dimple/protrusion. The overall average Nusselt number on the tip wall with pin-fin-dimple/protrusion was increased by 31.2%–127.3% comparing to that of smooth tip wall. The mounting of dimple/protrusion and pin-fin-dimple/protrusion on the tip surface inside the blade could enhance the heat transfer with little increase of friction. Eren et al. [10] studied heat transfer characteristics and pressure drop in a rectangular channel by mounting cylindrical grooved pin-fins (C-GPFs) and triangular grooved pin-fins (T-GPFs) in inline and staggered array. Reynolds numbers and grooved distance ratio (b/e) considered ranged from 3,188 to 15,146 and 1 to 3.446, respectively. The result showed that enhancement of thermal performance with mounting cylindrical grooved pin-fins and triangular grooved pin-fins on heat transfer surface. For case T-GPFs and C-GPFs, the maximum heat transfer rate was obtained in in-line and staggered array with Reynolds number at 15,146, b/e ratio at 3.446. The thermal performance for the C-GPFs and T-GPFs was found to be the best and was about 2.27 and 2.81, respectively.

Lawson et al. [11] presented the effects of spanwise and streamwise spacing of straight pin to heat transfer rate and pressure loss for a range of Reynolds between 5,000 and 30,000. Reduction of pin spacing for spanwise and streamwise increased the heat transfer due to increasing of flow acceleration. Heat transfer enhancement of straight pin was found higher for less streamwise pin spacing than less spanwise pin spacing. The friction factor of straight pin was higher for spanwise pin spacing than streamwise pin spacing with flow blockage. Chyu et al. [12] study heat transfer on convective surfaces with pin arrays mounted in inclined angles ($40^o$, $60^o$ and $75^o$) which compared to case of straight pins configuration. Small inclined angles ($40^o$, $60^o$, $75^o$) of pin arrays did not have effect on increasing heat transfer and it reduced pressure drop in channel when compare to case straight pins. The thermal performance was highest in case straight pins. Takeishi et al. [13] studied heat transfer characteristics and pressure loss of normal and inclined pins arrayed in rectangular duct with flat and wavy endwall. The angle pins ($-45^o$, $0^o$, and $+45^o$) with flat endwall and a $-45^o$ angled pin with wavy endwall were tested. The average heat transfer coefficient of $-45^o$ inclined pins with wavy endwall is the same that of normal pins with flat endwall, but the pressure drop for case of $-45^o$ inclined pins with wavy endwall was less than that of normal pin-fins with flat endwall. Choi et al. [14] investigated the influence of pin inclination angle on heat transfer surface and flow field around a cylinder.

Fig.1. shows the schematic diagram of flow features around the inclined cylinder. The heat transfer on the upper end wall is enhanced due to the impingement of the interaction between the horseshoe vortex and the jet-like flow. However, the heat transfer on the lower end wall is reduced due to the wake region behind the inclined cylinder. The variation in angle of pin arrays shown in the literature suggested that the angle of inclined pin has a large effect on pressure drop.

For the current study, experiments were conducted at constant Reynolds number Re=5,200 to explore the effects of angle inclined pin on heat transfer and flow characteristics with H/D=2. The height of pin was fixed at 62.5% from

the height of channel. The objective of this study was to investigate the flow and heat transfer characteristics on a row of inclined cylindrical pin's surface. The effects of pin inclination angle to heat transfer surface were investigated for $\theta = 30^o$, $45^o$, $60^o$, $90^o$, $120^o$, $135^o$, and $150^o$. All experiments were performed at constant Reynolds number Re=5,200 for comparing the results.

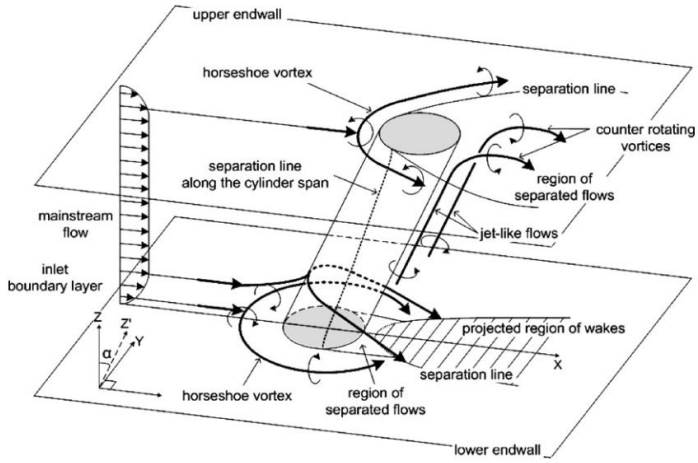


**Fig.1.** Schematic diagram of flow features around an inclined cylinder [14].

## 2. EXPERIMENTAL SETUP

The details of experimental model are shown in Fig.2. A row of cylindrical pins having diameter of D=10 mm are mounted in spanwise direction in wind tunnel with normal to flow direction. The pin height (H) and pin-to-pin distance (S) are fixed at H=2D and S=2D, respectively. The height of pin was fixed at 62.5% from the height of channel. The origin of the Cartesian coordinates is located at center of the central pin in the row. The X, Y and Z axes are fixed on streamwise, spanwise and normal to the heat transfer wall in wind tunnel. The heat transfer surface has length of 27D and width of 18D. In this work, the effects of pin inclination angle of pins were investigated for $\theta = 30^o$, $45^o$, $60^o$, $90^o$, $120^o$, $135^o$ and $150^o$.

A schematic diagram of the experimental apparatus is show in Fig. 3. The air flow was introduced through the wind tunnel passing inlet section, test section and air chamber using blower as indicated in Fig. 3. The wind tunnel has rectangular cross section with dimension of 300×32 $mm^2$. The wind tunnel can be divided into three parts**;** upstream section (before test section), test section, and downstream section (after test section). The upstream section with 1,535 mm ($26.6D_h$) of length has a sufficient length to provide a fully developed flow before entering the test section. The test section with 270 mm ($4.7D_h$) of length was with heat transfer measurement. The pressure drop was measured in the test section. The downstream section of 533 mm ($9.2D_h$) length was connected with wind tunnel to air chamber with an orifice flow meter and blower. A pitot-static tube was located at the center of the wind tunnel in upstream section to measure flow velocity. In this study, the Reynolds number based on the center velocity and pin diameter was fixed at Re= 5,200 for all experiments. The inlet temperature of the air flow was kept constant at $25 \pm 0.5^o$C.

The details of heat transfer surface of test section are also shown in Fig.3. The heat transfer surface was made of a stainless steel foil with thickness of 30-$\mu$m. The stainless steel foil was stretched between couples of copper bus bars. The heat transfer surface was heated by supplying electrical current via a DC power source through the copper bus bar. For temperature measurement, a thermochromic liquid crystal (TLC) sheet was attached on the rear side of heat transfer surface. The TLC sheet indicated the color change for temperature $30^o$C to $35^o$C. The correlation between color and temperature was developed by calibration with some thermocouples under experimental conditions to keep same measuring environment such as lighting. The color information from TLC sheet was then converted to temperature using image processing technique.

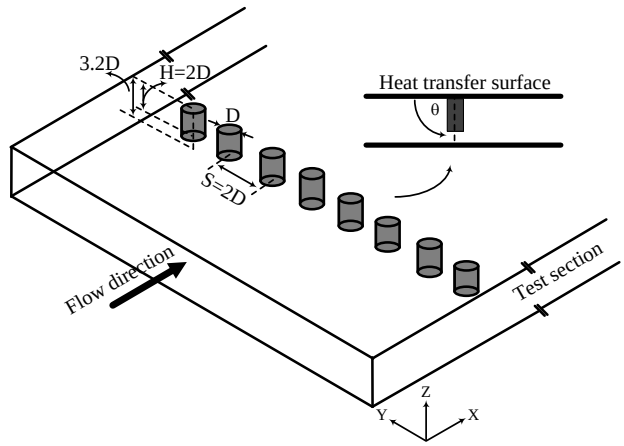


**Fig.2.** Experimental model of pins in test section.

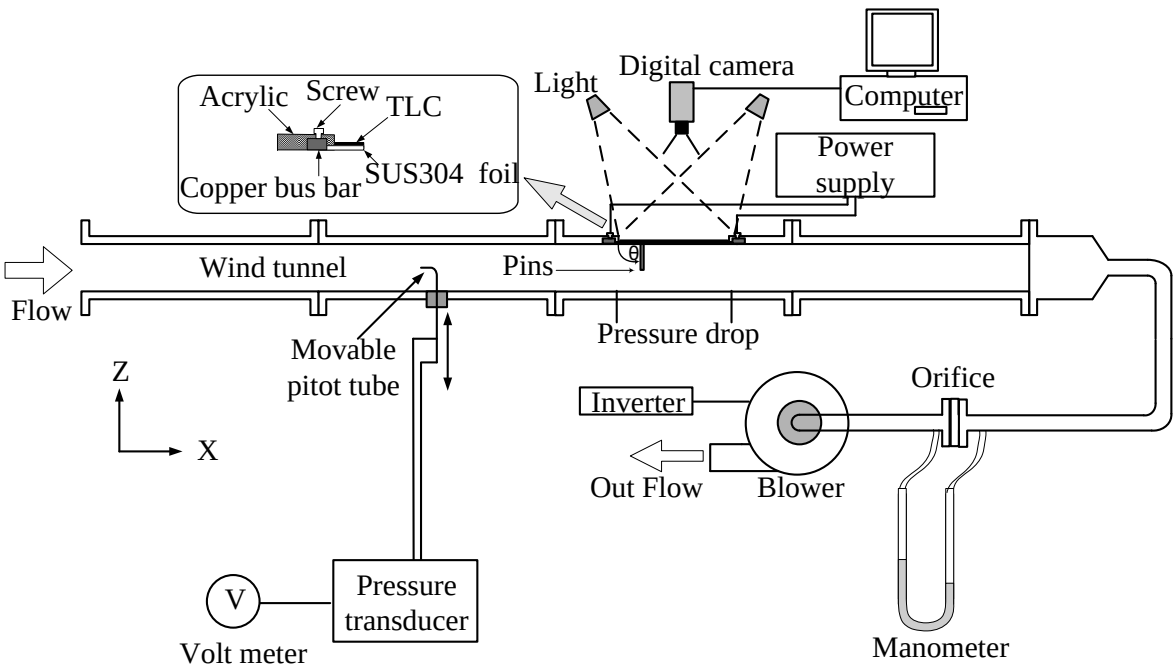


**Fig.3.** Schematic diagram of experimental setup.

### 3. DATA PROCESSING

The local heat transfer coefficient under forced convection can be evaluated as:

$$\dot{Q}_{input} = I^2 R \tag{1}$$

$$\dot{Q}_{losses} = \dot{Q}_{conv} + \dot{Q}_{rad} \tag{2}$$

$$h = \frac{\dot{Q}_{input} - \dot{Q}_{losses}}{(T_w - T_a)A} \tag{3}$$

Where $I$, $A$ and $R$ are the electrical current, the heat transfer area on stainless steel foil and the resistance of the stainless steel foil. The wall temperature ($T_w$) on heat transfer surface is obtained using TLC sheet (color information). $T_a$ is air flow temperature measured at upstream of test section.

$\dot{Q}_{conv}$ and $\dot{Q}_{rad}$ are the mean heat losses from the rear side of TLC sheet to the surrounding by radiation and free convection calculated from:

$$\dot{Q}_{conv} = h_c A_{loss}(\overline{T}_w - T_s) \tag{4}$$

$$\dot{Q}_{rad} = \sigma \varepsilon_{TLC} A_{loss}(\overline{T}_w^4 - T_s^4) \tag{5}$$

Where $h_c$ is the natural convection coefficient from hot horizontal plate obtained by equation of natural convection [15], $\overline{T}_w$ is average wall temperature and $T_s$ is surrounding temperature, $A_{loss}$ is area of TLC sheet to the surrounding on the rear side of heat transfer surface, $\sigma$ is the Stefan-Boltzmann constant and $\varepsilon_{TLC}$ is the emissivity coefficient of TLC sheet at 0.9 [16]. The local Nusselt number can be calculated as:

$$Nu = \frac{hD}{k} \tag{6}$$

Where, $D$ and $k$ are the diameter of pin and thermal conductivity of air. The Reynolds number can be calculated as:

$$Re = \frac{V_c D}{\upsilon} \tag{7}$$

Where, $V_c$ is the air velocity at the center of wind tunnel in upstream section. The method of experimental uncertainty by Kline and McClintock [17] was studied for error analysis. The Nusselt number uncertainty is between 2.61% and 4.63%, and the uncertainty of friction factor is between 4.36% and 4.82% [18].

## 4. NUMERICAL METHOD

The three dimensional governing equations for continuity, momentum, and energy are as follows [19-21].

### *4.1 Continuity equation*

$$\frac{\partial \rho u_i}{\partial x_i} = 0 \tag{8}$$

### *4.2 Momentum equation*

$$\rho u_j \frac{\partial u_i}{\partial x_i} = \frac{\partial}{\partial x_j}\left[(\mu + \mu_t)\frac{\partial u_i}{\partial x_j}\right] - \frac{\partial p}{\partial x_i} \tag{9}$$

### *4.3 Energy equation*

$$\rho u_j \frac{\partial T_i}{\partial x_i} = \frac{\partial}{\partial x_j}\left[\left(\frac{\mu}{Pr} + \frac{\mu_t}{Pr_t}\right)\frac{\partial T}{\partial x_j}\right] \tag{10}$$

The numerical simulation with ANSYS ver. 14 (FLUENT) was used to solve Reynolds Averaged continuity equation, Navier-Stokes equations and energy equation for obtaining three dimensional flow field and heat transfer on the surface. The solution method for obtaining velocity and pressure field was based on Semi-Implicit Method for Pressure-Linked Equations (SIMPLE) algorithm with second order upwind for all spatial discretization. The turbulence flow was analyzed using shear-stress-transport SST k-$\omega$ turbulence model. The SST k-$\omega$ model combines the advantages of the k-$\varepsilon$ and k-$\omega$ models with a blending function. Kim and Moon [22] applied the SST k-$\omega$ model to predict the numerical model for enhance the heat transfer performance by a stepped circular pin fin array. The SST k-$\omega$ model was given the good prediction for problem of flow with adverse pressure gradient and separation zones [23, 24]. Garg and Ameri [25] found that the SST k-$\omega$ model resolved the passage vortex better than two-equation k-$\omega$ model of heat transfer on turbine blade. The simulation result with SST k-$\omega$ model, for pin fins and plate fins shows that the separation bubbles and the turbulence generation behind the circular pins were much larger than plate fins [26]. The root mean square (RMS) residual of continuity and energy equation is less than $10^{-5}$ and that of momentum equation is less than $10^{-4}$, the computed domain is considered for convergence.
To validate the grid system, grid dependency test was performed and compared the velocity profile distribution in the Z-axis after test section for $\theta = 30^{o}$ as shown in Fig.4. It can be noticed that the trend of velocity profile for grid number at 2,648,700 and 3,505,572 displays less discrepancy than others cases. The meshes with approximate 2,648,700 grids were chosen for simulation. The Nusselt number distributions for different pin inclination angles with simulation are shown in Fig.5. The trends of Nusselt number contours of simulation in Fig.5 were same as experiment in Fig.6. The values of Nusselt number from simulation (Fig.5.) and experimental (Fig.6.) are less different with comparing to that of other works [27, 28].

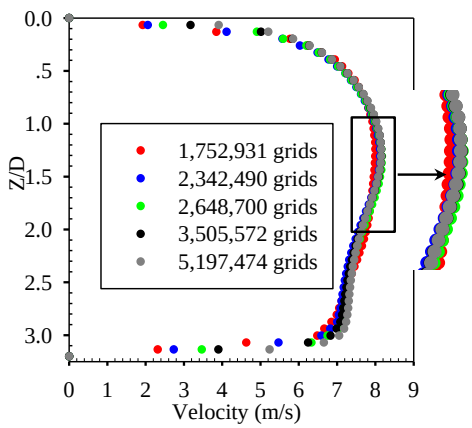


**Fig.4.** Grid dependency test with velocity distribution for $\theta = 30^{o}$.

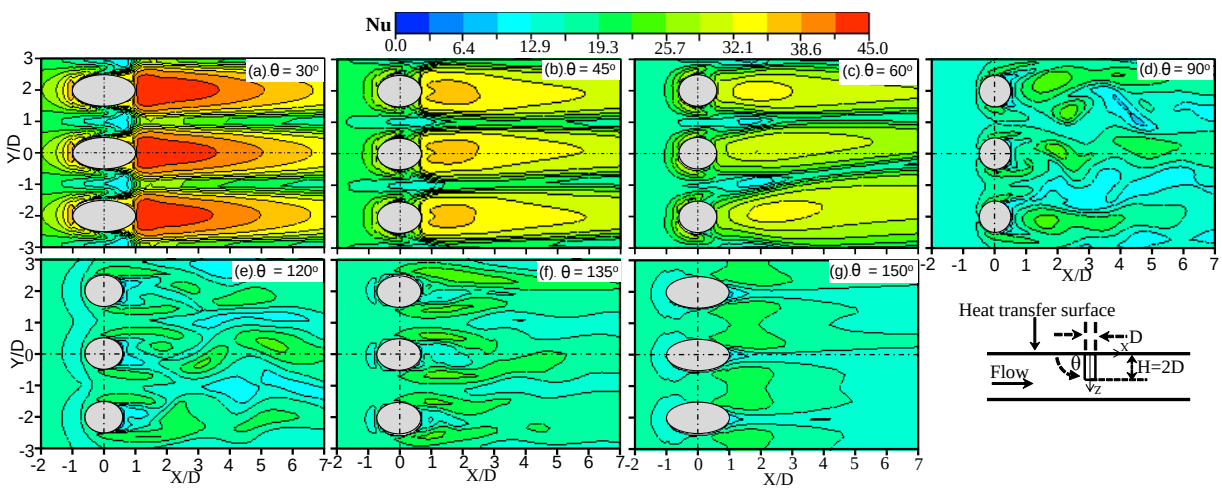


**Fig.5.** Nusselt number distributions for different pin inclination angles obtained from simulation.

## 5. RESULTS AND DISCUSSION

### *5.1 Local Nusselt number*

Nusselt number contour (for three pitches of pins in the center on heat transfer surface) using TLC sheet are shown in Fig.6. The air flows from left hand to right hand side in each result. It can be seen from the contours, the local Nusselt number for $\theta = 90^o$ is high for small area in upstream region near the front of pin. This is due to the effect of horse shoe vortex around the pin near heat transfer surface. While, the Nusselt number in down steam region is higher and covers large area. The obtained results show almost similar trends with other studies [11, 29 and 30].
The local Nusselt number with increasing of pin inclination angle $\theta = 30^o$, $45^o$, $60^o$ and $90^o$ in upstream region tends to decrease and in downstream region it also tends to decrease Nusselt. The maximum and minimum Nusselt number obtained for pin inclination angle $\theta = 30^o$ and $\theta = 90^o$, respectively. The inclined pin for $\theta = 30^o$ gives the largest heat transfer enhancement for both upstream and downstream of pin row.

For pin inclination angle $\theta = 120^o$, $135^o$ and $150^o$, the local Nusselt number in upstream of pins tends to decrease when increase the pin inclination angle from $\theta = 90^o$ to $120^o$, $135^o$ and $150^o$. The local Nusselt number in downstream of pins increased a little when increase the pin angle from $\theta = 90^o$ to $120^o$ and $135^o$. But, the local Nusselt number in downstream of pin deceases and get smaller for $\theta = 150^o$ than $\theta = 90^o$. It was ascertained that the pin inclination angle has strong effect on end wall heat transfer with pin attachment. Fig. 7 and Fig. 6 represent the local Nusselt number along the X axis. The local Nusselt number was not shown for region of heat surface under the pin.

For pin angle $\theta = 90^o$, the local Nusselt number in upstream region tends to increase as going close to the pin. In downstream region, the local Nusselt number tends to increase from pin and become maximum value at X/D=2, then the local Nusselt number gradually decreases as going to downstream.
For pin inclination angle $\theta = 30^o$, $45^o$ and $60^o$, the local Nusselt number tends to comparatively increase and for downstream of pin tends to increase rapidly when it was compared with $\theta = 90^o$. The location of maximum Nusselt number has shifted from X/D= 2 to X/D $\approx$1.

For pin inclination angle $\theta = 120^o$, $135^o$ and $150^o$, the local Nusselt number was almost same with case of $\theta = 90^o$. The local Nusselt number in downstream of pin for $\theta = 120^o$ and $135^o$ slightly increased as compared to case of $\theta = 90^o$ whereas, for case of $\theta = 150^o$ it was relatively low behind the pin. The mechanism of heat transfer enhancement and deterioration is also explained using CFD simulations.

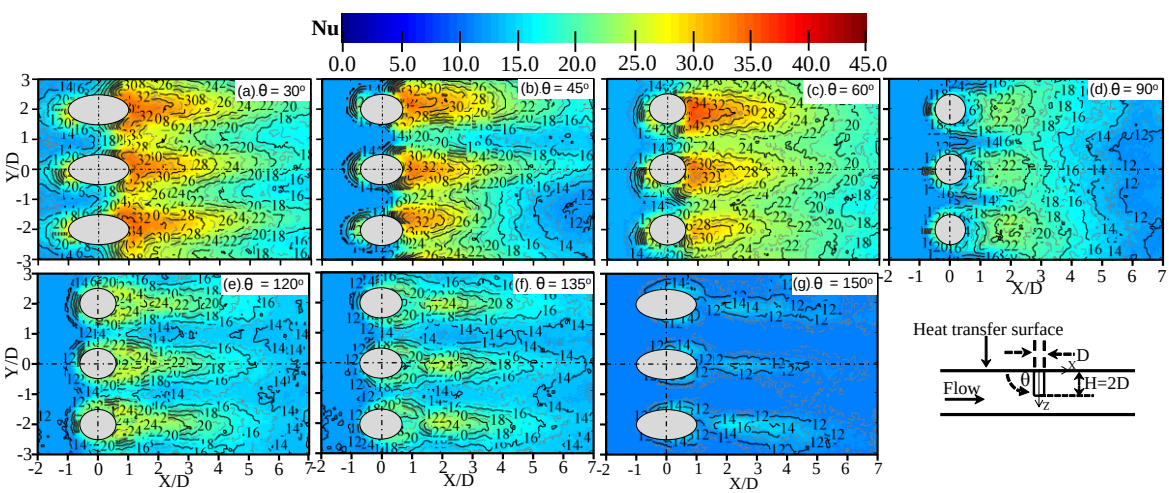


**Fig.6.** Nusselt number distributions for different pin inclination angles.

Spanwise average Nusselt numbers along the downstream direction are plotted in Fig. 8 for comparison the effect of pin inclination angle. This spanwise average Nusselt number was calculated by averaging the local Nusselt number at different X distances. The local Nusselt numbers under the pins was not considered for calculation. The trends of spanwise average Nusselt number were same as the results of local Nusselt number along X-axis at Y/D = 0. The pin inclination angle $\theta = 30^o$ shows the highest spanwise average Nusselt number in upstream and downstream region of pins. While, pin inclination angle $\theta = 150^o$ gives the lowest Nusselt number.

*5.2 Overall average Nusselt number*

The overall average Nusselt number for all of pin inclination angle is plotted in Fig. 9. This overall average Nusselt number is calculated by averaging the local Nusselt number obtained from Fig. 6. Fig. 10 shows the percentage of increasing overall average Nusselt numbers as compared to $\theta = 90^o$. The pin inclination angle $\theta = 30^o$, $45^o$ and $60^o$ can enhance the overall average Nusselt number about 40.1%, 21.97% and 38.4% as compared to pin angle $\theta = 90^o$. On the other hand, the pin inclination angle $\theta = 120^o$ and $135^o$ can somewhat improve the overall average Nusselt number about 6.58% and 1.11%, respectively. The pin inclination angle $\theta = 150^o$ gives lower average Nusselt number about 24.32% as compared to $\theta = 90^o$.

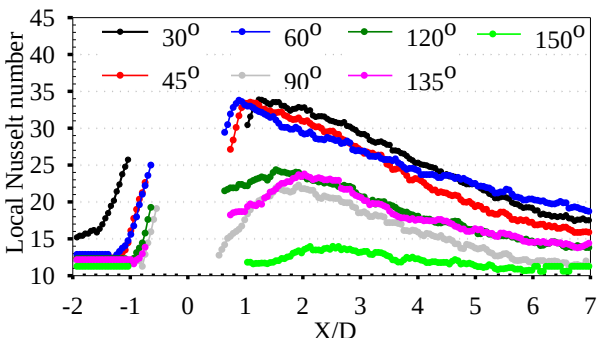


**Fig.7**. Local Nusselt number along X-axis at Y/D=0 for different pin inclination angles.

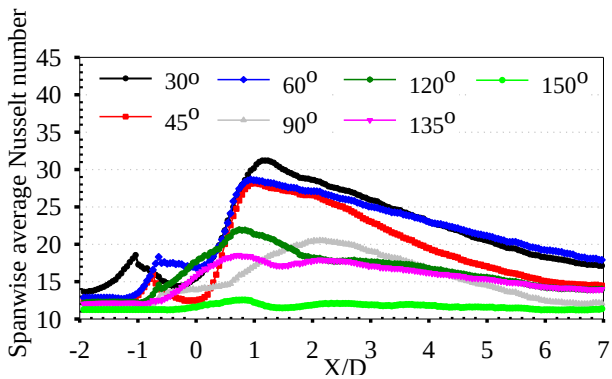


**Fig.8**. Spanwise average Nusselt number along X-axis for different pin inclination angles.

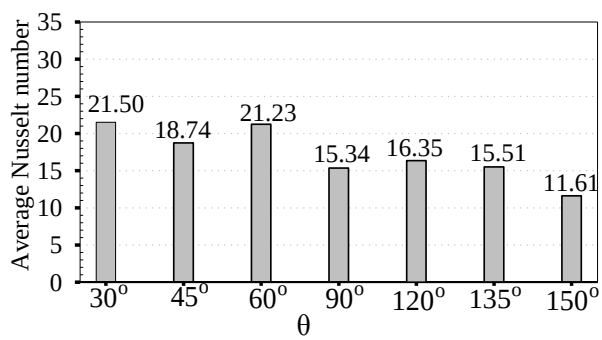


**Fig.9**. Average Nusselt number for different pin inclination angles.

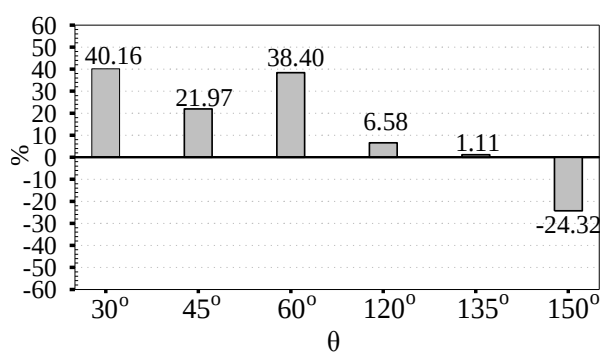


**Fig.10**. Increasing percent of average end wall Nusselt number for different pin inclination angles as compared to $\theta = 90^o$.

*5.3 Flow Patterns*

Fig. 11 compares the behavior of flow in terms of streamline on X-Y plane at 1 mm below the heat transfer surface. To obtain the results, CFD simulation has been performed for different pin inclination angles. In the figures, the air flows from left hand to right hand passing a row of pins.

For pin inclination angle $\theta = 30^o$, $45^o$ and $60^o$, there were two acceleration flow regions located near the front of pin for each pins. There are also footprints two counter rotating vortices between the downstream of pins. The velocity in downstream region of each pin will be increased due to the interaction of two rotating vortices. This flow characteristic promotes the heat transfer behind the pins. Counter-rotating vortices in downstream of these inclined pin can destroy the wake flow behind the pins.

For pin inclination angle $\theta = 90^o$, there were footprint of two wake flows behind each pins. The velocity near the heat transfer surface becomes small behind the pins. For pin inclination angle $\theta = 120^o$ and $135^o$, the footprint of wake flows can be also found behind the pin. But the area of low velocity region becomes small as compared to case of pin angle $\theta = 90^o$.

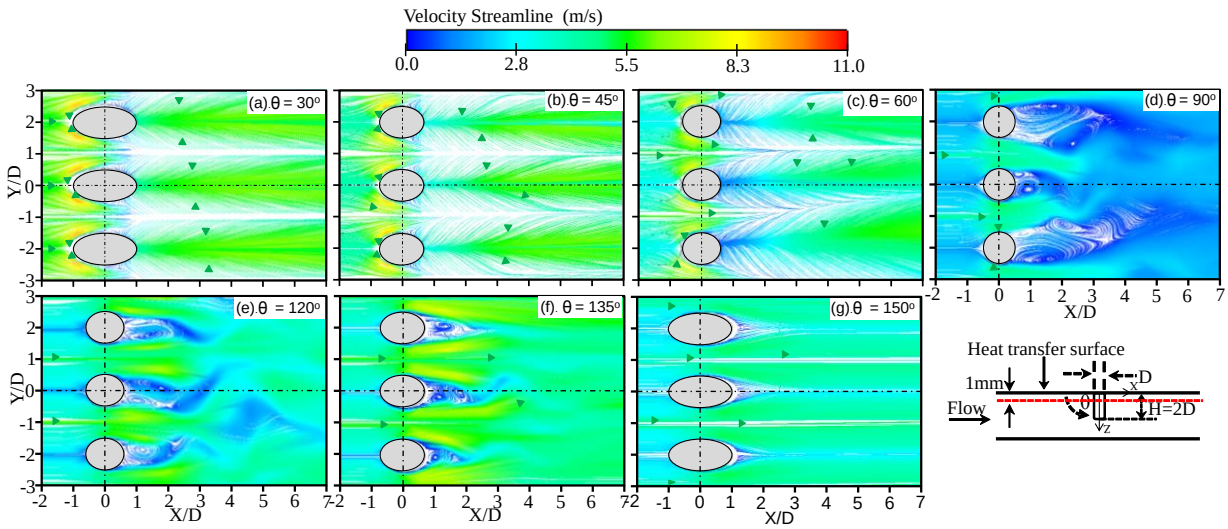


**Fig.11**. Streamlines on the X-Y plane near the heat transfer surface (1.0-mm below the heat transfer surface) of inclined pins.

For pin inclination angle $\theta = 150^o$, the low velocity region was seen behind the each pin and it extended to far downstream. The low velocity region causes to decrease the heat transfer behind the pins. However, the oscillating wakes flow for pin inclination angle $\theta = 120^o$ and $135^o$ can disturb the boundary flow behind the pins. This result promotes the heat transfer on surface as compared to $\theta = 90^o$ and $150^o$.

Fig. 12 shows the velocity contour on Z-X plane passing the pin center obtained from CFD results compared with different pin inclination angles. The low velocity region behind the pin detected for case of pin angle $\theta = 90^o$, $120^o$ and $135^o$. This region corresponds to wake flow region behind the pin. However, the low velocity region cannot be seen for $\theta = 30^o$ and $45^o$, while, it can be found near the heat transfer wall and on the rear of pin for case of $\theta = 60^o$ and $150^o$, respectively.

Fig. 14 shows the velocity streamline on Y-Z plane at different locations as X/D=0, 1, 3 and 5. The results show the velocity regions of 4 pitches of pins in spanwise direction. For pin inclination angle $\theta = 30^o$, $45^o$ and $60^o$, there are a pair of counter-rotating vortices behind each pins on Y-Z plane at X/D=0. These vortices induce air flow impinging on the heat transfer surface in downstream region of pins. The air flow from the adjacent pin collides on the heat transfer wall (spanwise direction) and then generate the secondary counter-rotating vortices in the downstream region between the pins as shown Fig. 14 (for X/D=1, 3 and 5). This secondary counter-rotating vortex attached on the heat transfer surface and it became larger along with downstream. The heat transfer enhancement in downstream pins was the results of the secondary vortices.

For pin angle $\theta = 90^o$, $120^o$ and $135^o$, the counter-rotating vortices were not found. The low velocity region was detected behind the pin instead of rotating vortices. For pin inclination angle $\theta = 150^o$, the counter-rotating vortices

was found behind the pin on Y-Z plane at X/D=3 and 5. The vortices were found near the edge of pin which was away from the heat transfer surface. Hence, it has small effect on heat transfer surface and the heat transfer on surface is smallest as compared to the other cases. The effect of counter-rotating vortices at near heat transfer surface are significantly in increasing turbulence flow that enhance heat transfer [14] on mounting inclined pin in flow channel, as shown in Fig. 13.

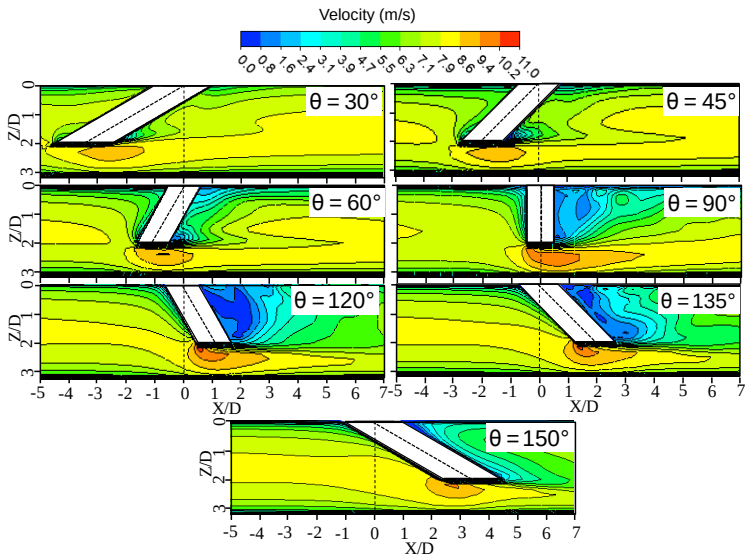


**Fig.12**. Comparisons of the streamwise velocity on Z-X plane passing the center of wind tunnel for various pin inclination angles.

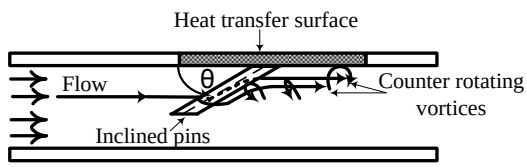


a. Counter rotating vortices near heat transfer surface, angle from 30º to 60º

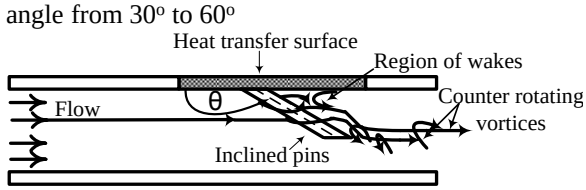


b. Counter rotating vortices far heat transfer surface, angle from 120º to 150º

**Fig.13**. Schematic diagram for explaining the air flow characteristics with mounting inclined pin on heat transfer surface.

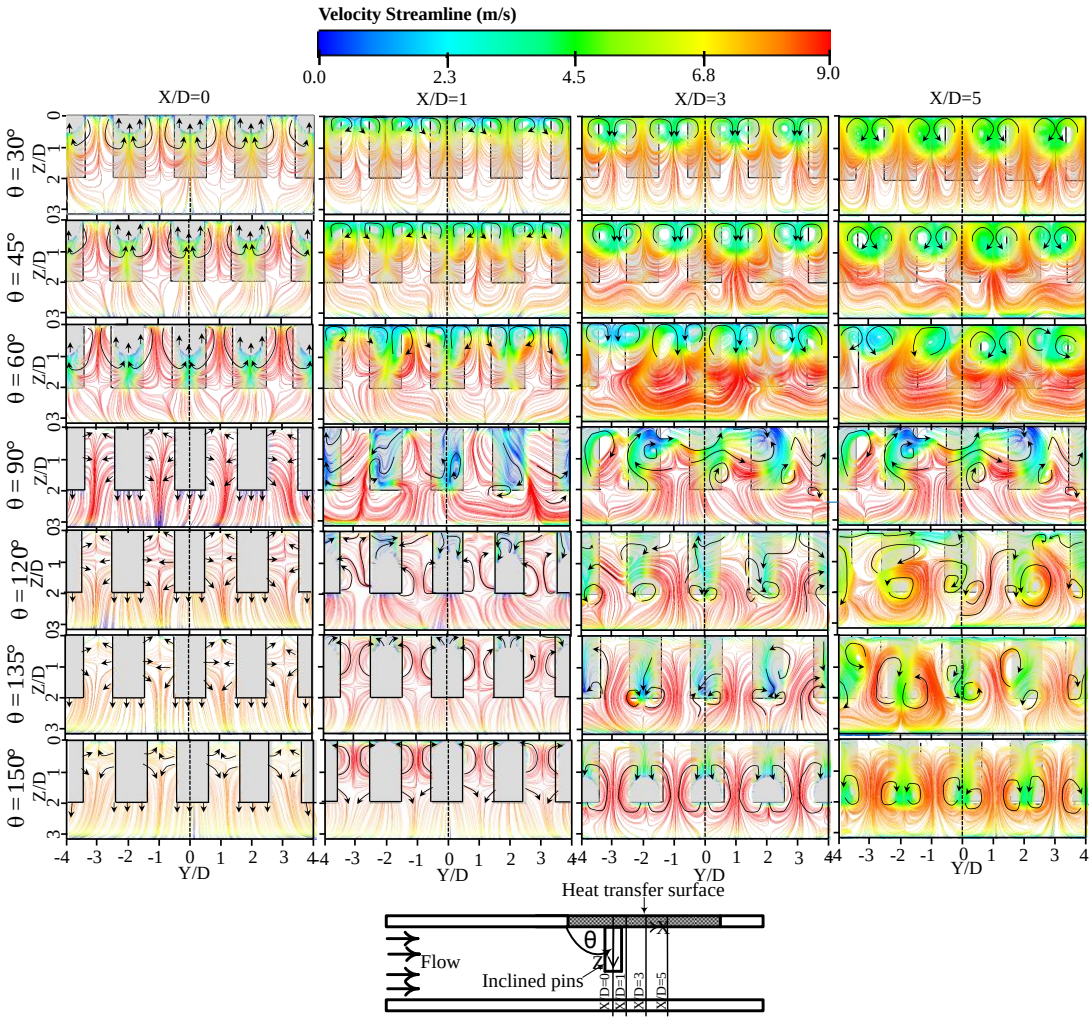


**Fig.14.** Comparisons of the streamlines on Y-Z plane with at some X/D for different pin inclination angles.

## 6. CONCLUSION

In this research work, the flow and heat transfer for a row of pins attached in wind tunnel was studied. The effects of pin inclination angles $\theta = 30^o, 45^o, 60^o, 90^o, 120^o, 135^o$, and $150^o$ were investigated. The height of pin was fixed at 62.5% from the height of channel. The main results obtained are as follows:

1. The pin inclination angle affected strongly heat transfer characteristics of surface of pins which was mounted in a row. The pin inclination angle $\theta = 30^o, 45^o, 60^o$ improved the heat transfer region in front of pins and it enhances the heat transfer behind pins. Particularly for case of $\theta = 30^o$, the overall average Nusselt number was found higher as 40.16% than $\theta = 90^o$.
2. The heat transfer for pin inclination angle $\theta = 120^o$ and $135^o$ slightly enhanced the behind the pins. However, the local Nusselt number decreases in upstream and downstream regions for respective pin angles. The overall average Nusselt number decreased about 24.3% for $\theta = 150^o$.
3. For pin inclination angle $\theta = 30^o, 45^o$ and $60^o$, a pair of counter-rotating vortices was generated behind each pins. These vortices introduced the secondary counter-rotating vortices in-between the pins near the heat transfer surface.
4. For pin angle $\theta = 90^o, 120^o$ and $135^o$, the wake with low velocity region detected behind each pins and this results low heat transfer region behind the pins.
5. The friction factor for pins with low pin inclination angle $\theta = 30^o, 45^o$ and $60^o$ was higher than the pins with angle $\theta = 90^o, 120^o, 135^o$ and $150^o$.

**NOMENCLATURE**

| | |
|---|---|
| A | heat transfer area, $m^2$ |
| D | pin diameter, m |
| $D_h$ | hydraulic diameter of wind tunnel (=0.0578 m), m |
| H | pin height, m |
| h | local heat transfer coefficient, $W/m^2$ K |
| I | electrical current, A |
| k | thermal conductivity, W/m K |
| L | length of test section, m |
| Nu | Nusselt number |
| $\Delta P$ | pressure drop in test section, Pa |
| R | electrical resistance, Ohm |
| Re | Reynolds number |
| S | pin-to-pin distance, m |
| T | temperature, $^\circ$C |
| V | velocity, m/s |

*Subscripts*

| | |
|---|---|
| a | air |
| c | center |
| conv | convection |
| h | hydraulic |
| rad | radiation |
| w | wall |

**REFERENCES**


[1] Lau, S. C., Kim, Y.S. and Han, J. C. Effects of fin configuration and entrance length on local endwall heat/mass transfer in a pin fin channel, ASME Paper 85-WA/HT-62, 1985.

[2] Chyu, M.K. and Natarajan, V. Heat transfer on the base surface of three-dimensional protruding elements, International Journal of Heat and Mass Transfer, Vol. 39(14), 1996, pp. 2925-2935.

[3] Zukauskas, A. A. Heat transfer from tube in cross flow, Advances in Heat Transfer, Vol. 8, 1972, pp. 116-133.

[4] Chyu, M.K. Heat transfer and pressure drop for short pin-fin arrays with pin-endwall fillet, ASME Journal of Heat Transfer, Vol. 112, 1990, pp. 926-932.

[5] Pandit, J., Thompson, M., Ekkad, S.V. and Huxtable, S.T. Effect of pin fin to channel height ratio and pin fin geometry on heat transfer performance for flow in rectangular channels, International Journal of Heat and Mass Transfer, Vol. 77, 2014, pp. 359-368.

[6] Rao, Y., Wan, C. and Xu, Y. An experimental study of pressure loss and heat transfer in the pin fin-dimple channels with various dimple depths, International Journal of Heat and Mass Transfer, Vol. 55, 2012, pp. 6723-6733.

[7] Wan, C., Rao, Y. and Chen, P. Numerical predictions of jet impingement heat transfer on square pin-fin roughened plates, Applied Thermal Engineering, Vol. 80, 2015, pp. 301-309.

[8] Axtmann, M., Poser, R., Wolfersdorf, J.V. and Bouchez, M. Endwall heat transfer and pressure loss measurements in staggered arrays of adiabatic pin fins, Applied Thermal Engineering, Vol. 103, 2016, pp. 1048-1056.

[9] Xie, Y., Shi, D. and Shen, Z. Experimental and numerical investigation of heat transfer and friction performance for turbine blade tip cap with combined pin-fin-dimple/protrusion structure, International Journal of Heat and Mass Transfer, Vol. 104, 2017, pp. 1120-1134.

[10] Eren, M. and Caliskan, S. Effect of grooved pin-fins in a rectangular channel on heat transfer augmentation and friction factor using Taguchi method, International Journal of Heat and Mass Transfer, Vol. 102, 2016, pp. 1108-1122.

[11] Lawson, S.A., Thrift, A.A., Thole, K.A. and Kohli, A. Heat transfer from multiple row arrays of low aspect ratio pin fin, International Journal of Heat and Mass Transfer, Vol. 54, 2011, pp. 4099-4109.

[12] Chyu, M.K., Oluyede, E.O. and Moon, H.-K. Heat transfer on convective surfaces with pin-fins mounted in inclined angles, Proceedings of GT2007, 2007, Montreal, Canada.

[13] Takeishi, K., Oda, Y., Miyake, Y. and Motoda, Y. Experimental and numerical study on the convective heat transfer and pressure loss in rectangular ducts with inclined pin-fin on a wavy endwall, Proceedings of ASME Turbo Expo, 2012, Copenhagen, Denmark.
[14] Choi, I. K., Kim, T., Song, S. J. and Lu, T. J. Endwall heat transfer and fluid flow around an inclined short cylinder, International Journal of Heat and Mass Transfer, Vol. 50, 2007, pp. 919-930.
[15] Incropera, F.P., Dewitt, D.P., Bergman, T.L. and Lavine, A.S. Introduction to Heat Transfer, Fifth Edition, John Wiley & Sons (2007).
[16] Wae-hayee, M., Tekasakul, P., Eiamsa-ard, S. and Nuntadusit, C. Effect of cross-flow velocity on flow and heat transfer characteristics of impinging jet with low jet-to-plate distance, Journal of Mechanical Science and Technology, Vol. 28, 2014, pp. 2909-2917.
[17] Kline, S.J. and McClintock. Describing uncertainties in single-example experiments, Mechanical Engineering, Vol. 75, 1953, pp. 3-8.
[18] Nuntadusit, C., Piya, I., Wae-hayee, M. and Eiamsa-ard, S. Heat transfer characteristics in a channel fitted with zigzag-cut baffles, Journal of Mechanical Science and Technology, Vol. 29, 2015, pp. 2547-2554.
[19] Anderson, J. D. Governing Equations of Fluid Dynamics, In Anderson, J. D., Degrez, G.E. and Degroote, J., et al. (eds.), Computational Fluid Dynamics, 3rd ed., chap. 2, Springer (2009).
[20] Baliga, B.R. and Atabaki, N. Control-Volume-Based Finite-Difference, and Finite-Element Methods, In Minkowycz, W.J., Sparrow, E.M. and Murthy, J.Y. (eds.), Hand-book of Numerical Heat Transfer, 2nd ed., chap. 6, Wiley (2009).
[21] Patankar, S. V. Numerical Heat Transfer and Fluid Flow, chap. 2, Hemisphere Publishing Corporation (1980).
[22] Kim, K.Y. and Moon, M.A. Optimization of a stepped circular pin-fin array to enhance heat transfer performance, Heat and Mass Transfer, Vol. 46, 2009, pp. 63-74.
[23] Mangani, L. and Bianchini, C. Heat transfer applications in turbomachinery, Proceedings of the OpenFOAM International Conference, 2007, ReinoUnido, London.
[24] Mangani, L., Bianchini, C., Andreini, A. and Facchini, B. Development and validation of a C++ object oriented cfd code for heat transfer analysis, Proceedings of the ASME–JSME thermal engineering conference and summer heat transfer conference (AJ-1266), 2007, Vancouver, Canada.
[25] Garg, V.K. and Ameri, A.A. Two-equation turbulence model for prediction of heat transfer on a transonic turbine blade, International Journal of Heat and Fluid Flow, Vol. 22, 2001, pp. 593-602.
[26] Carosio, G.L.C. and de Mendonca, M.T. Lower pressure drop turbine blade trailing-edge cooling configuration, Journal of the Brazilian Society of Mechanical Sciences Engineering, Vol. 37, 2015, pp. 1217-1233.
[27] Siw, S., Chyu, M.K., Shih, T.I-P., and Alvin, M.A. Effects of pin detached space on heat transfer and pin-fin arrays, ASME Journal of Heat Transfer, Vol. 134, 2012, pp. 1-9.
[28] Chi, X., Shih, T.I-P., Bryden, K.M., Siw, S. Chyu, M.K., Ames, R, and Dennis, R.A., Effects of pin-fin height on flow and heat transfer in a rectangular duct, Proceedings of ASME Turbo Expo (GT2011), 2011, Vancouver, British Columbia, Canada.
[29] Wang, F., Zhang, J. and Wang, S. Investigation on flow and heat transfer characteristic in rectangular channel with drop-shaped pin fins, Propulsion and Power Research, Vol. 1(1), 2012, pp. 64-70.
[30] Chang, S.W., Yanng, T.L. Huang, C.C. and Chiang, K.F., Endwall heat transfer and pressure drop in rectangular channels with attached and detached circular pin-fin array, International Journal of Heat and Mass Transfer, Vol. 51, 2008, pp. 5247-5259.